# Electrochemical characterization of NiO electrodes deposited via a scalable powder microblasting technique

Muhammad Awais [a, b, c], Danilo Dini [a, d], J.M. Don MacElroy [a, e], Yvonne Halpin [f], Johannes G. Vos [a, f], Denis P. Dowling [a, b, e]

a Solar Energy Conversion Strategic Research Cluster, Dublin

b School of Mechanical and Materials Engineering, University College Dublin, Ireland

c Interdisciplinary Research Centre in Biomedical Materials (IRCBM), COMSATS Institute of Information Technology (CIIT), Defence Road, Off Raiwind Road, Lahore, Pakistan

d Dept. of Chemistry, University of Rome "La Sapienza", Rome, Italy email: danilo.dini@uniroma1.it

e School of Chemical and Bioprocess Engineering, University College Dublin, Ireland

f School of Chemical Sciences, Dublin City University, Ireland

In this contribution a novel powder coating processing technique (microblasting) for the fabrication of nickel oxide (NiOx) coatings is reported. ~1.2 μm thick NiOx coatings are deposited at 20 mm2 s−1 by the bombardment of the NiOx powder onto a Ni sheet using an air jet at a speed of more than 180 m s−1. Microblast deposited NiOx coatings can be prepared at a high processing rate, do not need further thermal treatment. Therefore, this scalable method is time and energy efficient. The mechano-chemical bonding between the powder particles and substrate results in the formation of strongly adherent NiOx coatings. Microstructural analyses were carried out using SEM, the chemical composition and coatings orientation were determined by XPS and XRD, respectively. The electroactivity of the microblast deposited NiOx coatings was compared with that of NiOx coatings obtained by sintering NiOx nanoparticles previously sprayed onto Ni sheets. In the absence of a redox mediator in the electrolyte, the reduction current of microblast deposited NiOx coatings, when analyzed in anhydrous environment, was two times larger than that produced by higher porosity NiOx nanoparticles coatings of the same thickness obtained through spray coating followed by sintering. Under analogous experimental conditions thin layers of NiOx obtained by using the sol–gel method, ultrasonic spray- and electro-deposition show generally lower current density with respect to microblast samples of the same thickness. The electrochemical reduction of NiOx coatings is controlled by the bulk characteristics of the oxide and the relatively ordered structure of microblast NiOx coatings with respect to sintered NiOx nanoparticles here considered, is expected to increase the electron mobility and ionic charge diffusion lengths in the microblast samples. Finally, the increased level of adhesion of the microblast film on the metallic substrate affords a good electrical contact at the metal/metal oxide interface, and constitutes another reason in support of the choice of microblast as low-cost and scalable deposition method for oxide layers to be employed in electrochemical applications.

**Keywords:** nickel oxide, microblast deposition, photoelectrochemistry, dye-sensitization, intercalation reactions

## Introduction

Nickel oxide ($NiO_x$ with $1< x < 1.5$) is a *p*-type semiconductor with wide band-gap ($E_g$ > 3.50 eV),[1] and is characterized by high chemical stability[2] and optical transparency in the configuration of thin film (thickness, $l$ < 2 μm).[3,4] The intrinsic *p*-type conductivity of $NiO_x$ is mainly related to its non-stoichiometric nature where $Ni^{3+}$ centers constitute the oxide defects through which holes are transferred.[5] Because of this interesting combination of electrical and optical properties, $NiO_x$ has been considered for energy storage applications,[6-8] in electrochromic devices as transparent electrode,[9-17] in optoelectronic devices as electron barrier,[18,19] for gas sensing,[20,21] and, more recently, in dye-sensitized solar cells (DSCs) as photoactive cathode.[22-35] The utilization of $NiO_x$ in such diverse applications has been accompanied by the development of various preparation methods and deposition techniques, aimed at producing $NiO_x$–based materials with variable chemical composition, electrical resistivity, compactness and morphology. Examples include electrochemical deposition,[36] chemical vapor[37] and bath deposition,[38] spray pyrolysis,[39,40] sol-gel method,[14,23,25,41] hydrothermal synthesis,[29,42] and sputtering.[32] In this contribution, we propose a novel approach for the preparation of technologically relevant $NiO_x$ coatings for photo-electrochemical purposes using a microblasting technique.[43,44] The deposition method is based on the processing of the powder that constitutes the material of the coating. The powder grains are entrained in an air-jet and then bombarded onto metallic substrates at ambient

temperature. The mechanical energy of the powder particles in the air-jet is large enough to induce the formation of chemical bonds between powder material and substrate. The resulting coatings are characterized by a strong adhesion to the substrate and, importantly, do not require a post-deposition thermal treatment.[45] The latter feature reduces considerably the costs of surface finishing and film processing. Amongst the commercial deposition techniques applying this and related processes are CoBlast[43,44] and ROCATEC®.[45] To our knowledge, this is the first study that investigates the potential of the microblast technique for the deposition of metal oxide coatings for photo-electrochemical purposes. The morphological, structural, compositional, electrochemical and photo-electrochemical characteristics of microblast $NiO_x$ samples are described and compared with those of $NiO_x$ nanoparticulate layers prepared by furnace sintering,[22] and with those of nanocrystalline $NiO_x$ films prepared via sol-gel methods as reported in the literature.[9b,12b,14b,15b] Specifically the objective of this work is to evaluate the photo-electrochemical performance of microblast $NiO_x$ coatings in the bare state and in the sensitized version with the dye Erythrosin B (ERY).[23,41]

## Experimental

*Deposition of $NiO_x$ coatings*

The $NiO_x$ coatings were deposited onto 0.15 mm thick nickel sheets. The area of $NiO_x$ deposits was 2 cm x 2 cm. Nickel sheets from BDH Chemical Ltd. (UK), were ultrasonically cleaned for 5 minutes in 2-propanol followed by acetone, prior to the deposition. The nickel oxide powder was purchased from Chengdu Shudu Nano-Science Co. Ltd. A HELOS particle size analyzer from Sympatec GmbH was used to determine the size distribution of nickel oxide nanoparticles in the powder. The powder particles were dispersed in water under magnetic stirring at 1200 rpm during the analysis. The $NiO_x$ coatings were deposited using grit blasting in a commercial microblasting system (EnBIO Cork, Ireland), which has been described previously.[43,44] In this study, a single microblast nozzle was arranged perpendicularly to the substrates in order to produce a direct blast zone. The nickel oxide powder was fed into the nozzle at a pressure of 90 psi, with the nozzle located at a distance of 10 mm from the substrate made of nickel. The blast head was moved at a speed of 10 mm $s^{-1}$ over the substrate in an x–y co-ordinate geometry at a rate of 20 $mm^2$ $s^{-1}$. The deposition of the $NiO_x$ coatings was performed on Ni sheets instead of the conductive transparent substrates of indium-doped tin oxide (ITO), or fluorine-doped tin oxide (FTO). This is because the high-speed of $NiO_x$ particles can remove the conductive layer of either ITO or FTO, on the glass substrates and, consequently, reduce their effectiveness in the process of charge transfer between coating and substrate. In addition, an oxide forming substrate like metallic Ni is required in microblast process to achieve mechano-chemical reaction between the substrate and powder particles.[43,44] In order to compare the properties of the $NiO_x$ coatings prepared by the microblasting technique,(Sample A), $NiO_x$ nanoparticulate coatings were also deposited using conventional powder spraying and sintering (Sample B).[22] In this method $NiO_x$ nanoparticles were deposited onto 0.15 mm thick nickel sheets (2 cm x 2 cm) using a spraying technique similar to that described previously by Halme *et al.*.[46] $NiO_x$ nanoparticles, with an average particle size of 50 nm (Sigma-Aldrich) were suspended in 2-propanol (20 mg/mL), and a loosely adherent particulate layer of $NiO_x$ coatings was spray- deposited onto a Ni sheet. Successive sintering of the sprayed coating of $NiO_x$ nanoparticles was achieved with furnace treatments carried out in air at 450 °C for 30 minutes[22] using a Carbolite Furnace (RHF 1200). The thermal treatment is necessary for connecting the $NiO_x$ nanoparticles and for warranting the electrical contact between nanoparticles and at the $Ni/NiO_x$ interface.

*Characterization equipment*

The cross sectional investigations of the $NiO_x$ coating were carried out using a FEI Quanta 3D FEG DaulBeam™ (FEI Ltd, Hillsboro, USA) focused ion beam/scanning electron microscope (FIB/SEM) system. Prior to SEM analyses, the deposited $NiO_x$ films were coated with platinum via sputtering using an Emitech K575X sputter coating unit. This was done in order to prevent surface charging by the electron beam. Crystal properties were determined using X-ray Diffraction (XRD) measurements. These were carried out using a Siemens D500 diffractometer operating at 40 kV and 30 mA with Cu Kα radiation in normal diffraction mode at the scan rate 0.2° $min^{-1}$. X-ray Photoelectron Spectroscopy (XPS) data were recorded using a Kratos AXIS 165 spectrometer with a monochromatic X-ray source (Al $K_\alpha$ 1486.58 eV). The XPS survey spectra were collected in the binding energy range 0-1400 eV. The surface roughness was measured with a WYKO NT1100 optical profilometer. $NiO_x$ coatings were modified with Erythrosin B (Sigma-Aldrich) by immersion in a 0.3 mM solution of the dye in 99.8 % ethanol for 24 hours at room temperature. Electrochemical investigations on sensitised $NiO_x$ were carried out in Ar atmosphere using a cell with a three-electrode configuration:[9,47] the $NiO_x$ coatings and dye-containing $NiO_x$ films were used as the working electrodes, whereas two Li rods (Sigma-Aldrich) were used as reference and counter electrodes.[47] The electrolyte used was 0.5 M $LiClO_4$ in anhydrous propylene carbonate (Fisher). The potential values are referenced to the $Li^+/Li$ couple. The electrochemical cells were assembled under Ar atmosphere inside a glove-box (Innovative Technology, Newburyport, Massachusetts, USA). An argon atmosphere was maintained with oxygen content below 10 ppm and water content below 5 ppm. Cyclic

voltammetries[48] were carried out with an electrochemical analyzer (model 604C) from CH Instruments (Austin, Texas, USA).

## Results and discussion

*Surface analysis of the coatings*

Prior to microblast deposition, the particle size distribution of nickel oxide powder was determined using a HELOS laser particle size system (Sympatec GmbH). As detailed in Figure 1, the largest portion of oxide particles had a linear size of ~7.5 µm. The SEM image of these particles is given in Figure 2.

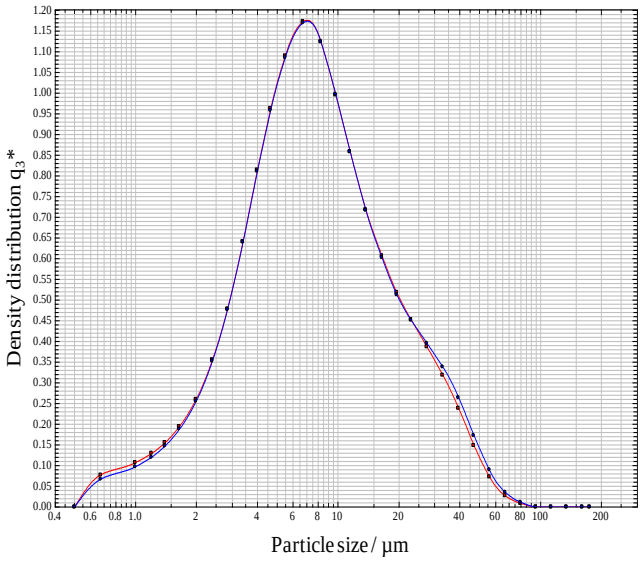


**Figure 1:** Particle size distribution of the nickel oxide powder used in the procedure of microblast deposition.

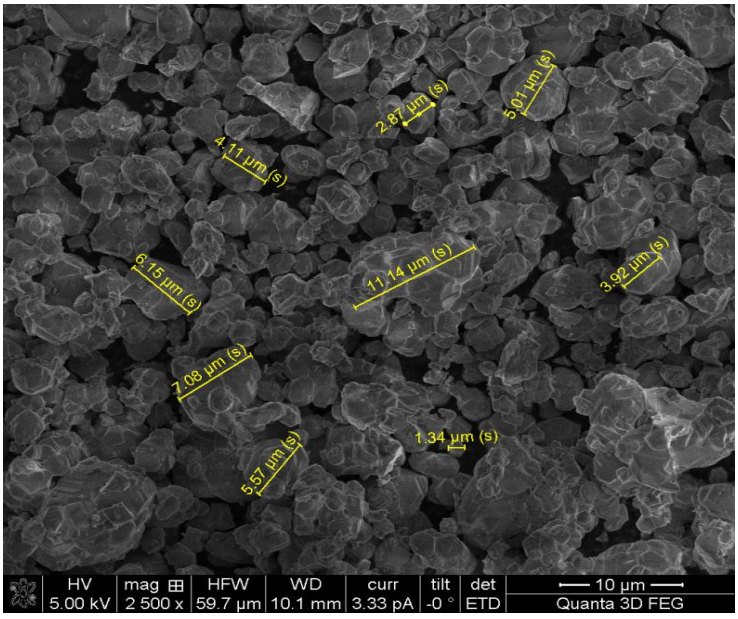


**Figure 2:** SEM image of the nickel oxide powder used in the microblast procedure. In the picture some particle diameters are shown to illustrate particle size range prior to microblast deposition.

Microblasting was carried out by blasting the nickel oxide powder entrained in an air jet onto Ni sheets at a velocity of about 180 m $s^{-1}$. The latter value was measured using a particle image velocimetry (PIV) system.[49] Upon impact with the Ni surface, the kinetic energy of the powder grains is converted partially into mechanical energy which induces

craters formation due to localized plastic deformation, and partially into potential energy which brings about chemical bond formation between the metallic substrate and the oxide particles.[45] Moreover, the impact of the micron-sized $NiO_x$ particles on the Ni substrate has a cleaning effect with the removal of the native oxide layer on the metal surface.[45] The mechanochemical reaction[50] between the powder particles and substrates enables the build-up of uniform $NiO_x$ layers on the Ni sheet as demonstrated in Figures 3 and 4.

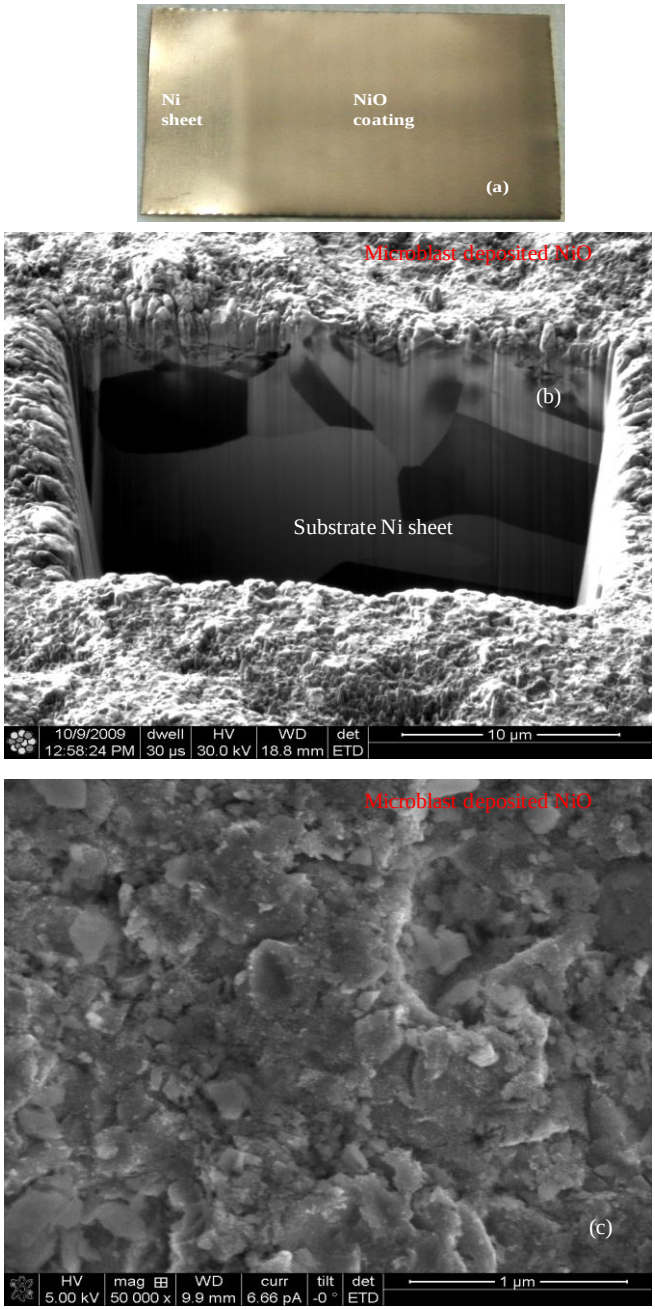


**Figure 3:**(a) Picture of the microblast deposited $NiO_x$ coatings on Ni sheet; (b) Cross-sectional FIB/SEM and (c) Topographic SEM images of the oxide coating.

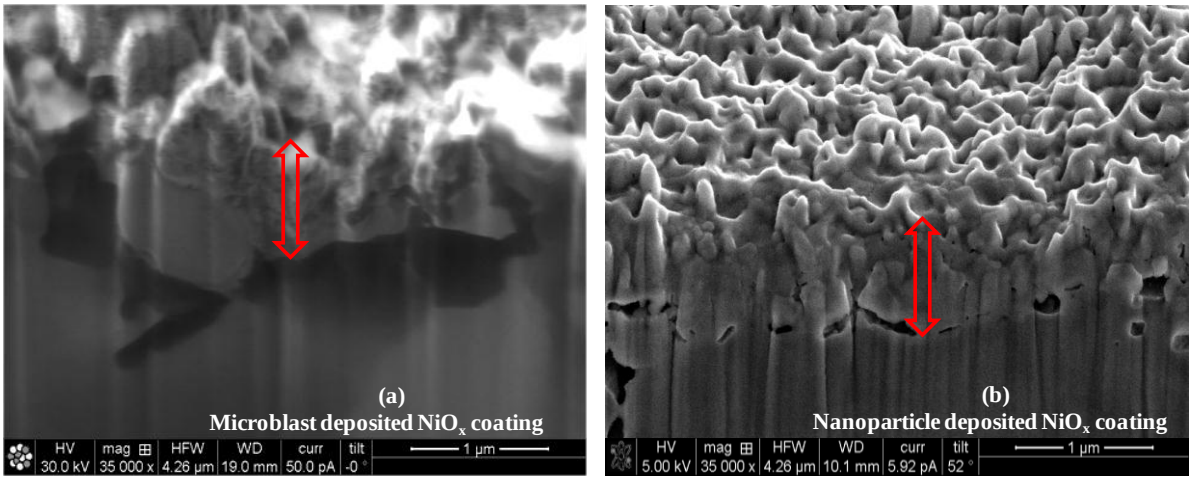


**Figure 4:** Cross sectional FIB/SEM images of $NiO_x$ coating on Ni sheet prepared via (a) microblast deposition of micron-sized grains of oxide, and (b) sintering of oxide nanoparticles with diameter of 50 nm. Samples thickness was ~1.2 µm (this is indicated with the red double-ended arrows in both pictures).

In the microblast procedure we have used deliberately □m size (see Figure 2) and not nm size oxide particles because the use of nanoparticles would have raised health and safety issues,[51] and because of a lack of sample containment in the microblast process. We are aware of the fact that it would have been more advantageous the use of nm size particles for obtaining thin film electrodes with larger surface area.[41] This issue is under further investigation. To benchmark the $NiO_x$ coatings prepared via the microblast technique (Sample **A**), we have also prepared $NiO_x$ films through the sintering [22] of spray deposited layers (Sample **B**) of $NiO_x$ nanoparticles on Ni sheets. Both microblast and nanoparticulate $NiO_x$ coatings have thickness values in the range of ~1.2 µm. It is evident that the microblast deposited coating (Figure 4a) exhibited lower levels of porosity compared with those deposited using the nanoparticles technique (Figure 4b). A summary of the physical properties of the $NiO_x$ coatings deposited using the microblast technique and the nanoparticles sintering route is given in Table 1.

| **Properties** | **Microblast deposited $NiO_x$** | **Nanoparticles $NiO_x$** |
|---|---|---|
| Nickel oxide particle size / µm | 7.5 | 0.05 |
| Thickness / µm | ~1.2 | ~1.2 |
| Coating roughness (Ra, Rq) / nm | ~ (400, 500) | ~ (400, 500) |
| Adhesion at Ni/$NiO_x$ interface | Good | Adequate |
| Heat treatment | No | Yes |

**Table 1:** Comparison of microblast and nanoparticles deposited $NiO_x$ coatings based on FIB/SEM cross-section images and surface roughness measurements.

*Crystal and chemical compositions of microblast deposited $NiO_x$ coatings*

The microblast deposited $NiO_x$ coatings were examined using XRD. The preferred surface orientations of both nickel oxide powder and microblast deposited $NiO_x$ coatings were the planes (111) and (200) (Figure 5).[21] The signature of the crystallographic plane (220) at 20~ 58 ° was not detected for the microblast $NiO_x$ coatings[21].

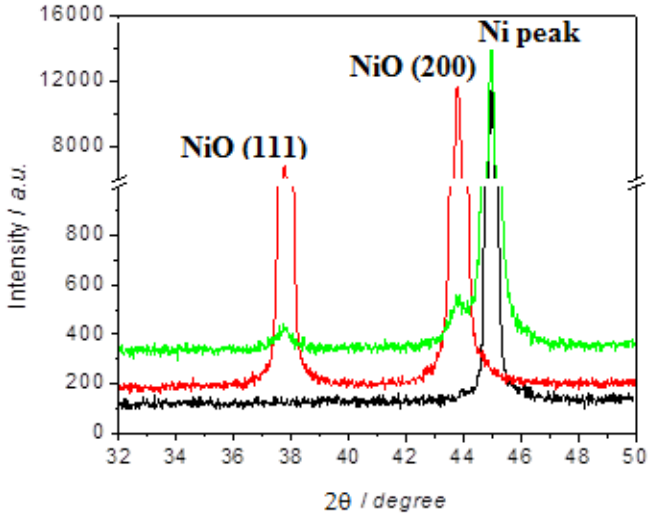


**Figure 5:** X-ray diffraction patterns of the Ni substrate (black trace), nickel oxide powder (red trace) and microblast deposited $NiO_x$ coating (green trace) onto Ni sheet.

The sintered films of $NiO_x$ nanoparticles displayed a XRD pattern (not shown in Figure 5) characterized by the signal associated with the $NiO_x$ (200) plane ($2\theta$ = 43.2 degrees). An XPS study was carried out to investigate the chemical composition of microblast deposited $NiO_x$ film and the coating obtained by sintering of $NiO_x$ nanoparticles (Figure 6). The Ni $2p_{3/2}$ spectra of Sample A coatings exhibit two peaks at 854 and 855.5 eV, which have been assigned to $Ni^{2+}$ (NiO) and $Ni^{3+}$ ($Ni_2O_3$) respectively (Figure 6-upper graph, blue profile).[52,53] This is in addition to the very broad peak at ~861 eV, which is the shake-up satellite peak of $Ni^{2+}$ and $Ni^{3+}$.[52,53] The complex peak structure makes it difficult the de-convolution of the peaks. However, the O1s spectra shown in Figure 6 (lower graph, blue profile) present two peaks at 529.4 eV and 531.4 eV, which are assigned to NiO and $Ni_2O_3$, respectively.[52,53]

The XPS spectra of the sintered layer of $NiO_x$ nanoparticles (Sample B) (Figure 6, red profiles) are characterized by the very broad feature of the emission in comparison to microblast $NiO_x$ signal (Figure 6, red profiles), whereas photoelectron emission energies fall in the same spectral region. these differences suggest an increased crystallinity in Sample A with respect to Sample B. In terms of chemical composition, also Sample B can be visualized as a mixture of NiO and $Ni_2O_3$, from the distinctive signatures of $Ni^{2+}$ and $Ni^{3+}$ in both Ni 2p and O 1s spectral regions (Figure 6, red profiles).[52]

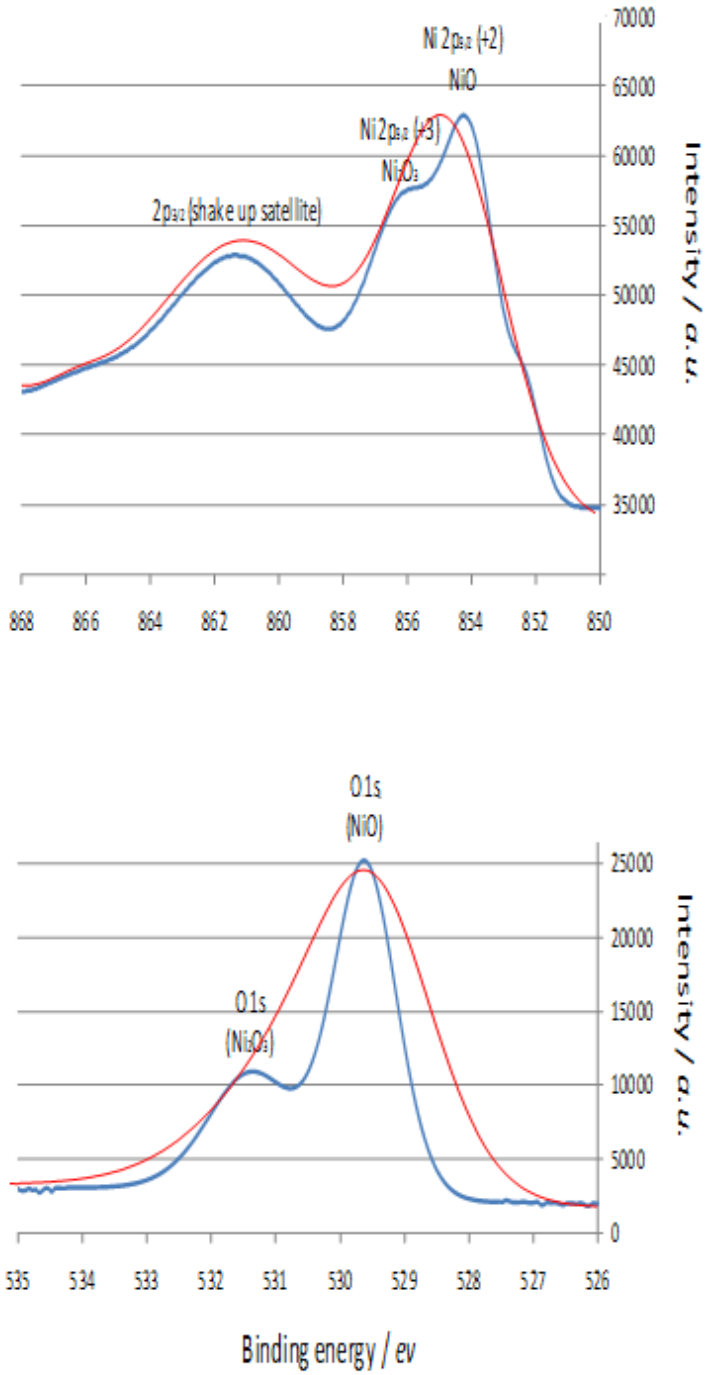


**Figure 6:** XPS spectra of (upper graph) Ni 2p and (lower graph) O 1s of microblast deposited (blue trace) and sintered (red trace) $NiO_x$ coatings.

*Electrochemical properties of microblast deposited $NiO_x$*

The $Ni/NiO_x$ interface of the microblast sample constitutes a metal/semiconductor junction that allows the passage of a cathodic current as verified when the applied external potential is less positive than 2.2 V *vs* $Li^+/Li$ in case (Figure 7).[47]

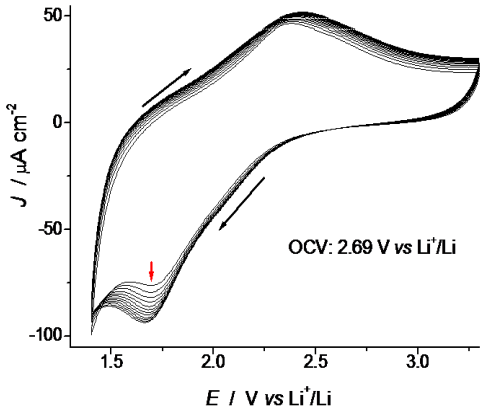


**Figure 7:** Cyclic voltammetry of a Sample A coating deposited on a Ni sheet. $NiO_x$ film thickness: 1.2 μm; electrolyte composition: 0.5M $LiClO_4$ in anhydrous propylene carbonate; scan rate: 40 mV $s^{-1}$. OCV stands for open circuit voltage. Black arrows indicate the direction of potential scan. The downward red arrow shows the direction of the variation of the cathodic current peak at 1.67 V *vs* $Li^+/Li$ upon continuous cycling.

This process corresponds to the injection of electrons into the $NiO_x$ film with resulting *n*-doping of the oxide. Charge injection in the semiconductor thin layer brings about the reduction of $NiO_x$ at 1.67 V *vs* $Li^+/Li$ according to the reaction [Eq. (1)]:[9]

$$NiO_x + ye^- + yLi^+ \Phi Li_yNiO_x \qquad (1)$$

The electrochemical cycling of a Sample **A** coating exhibits a continuous increase in the cathodic current peak at 1.67 V *vs* $Li^+/Li$ during the first 70-80 cycles (Figure 7). This study was carried out at a scan rate of 40 mV $s^{-1}$ and within a potential window of 1900 mV. These findings are consistent with what has been previously reported for thin $NiO_x$ layers undergoing repetitive cycles of electrochemical $Li^+$ ions insertion (intercalation)/removal.[9a,32,47] The increase in cathodic current is ascribed to the widening of the diffusion channels in the electrode structure through which lithium cation is exchanged.[14b,54] An analogous electrochemical behaviour was observed for the Sample **B** coatings (Figure 8).

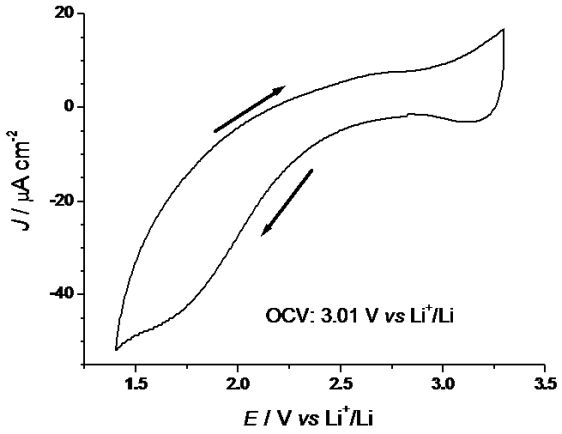


**Figure 8:** Cyclic voltammetry of Sample B coatings on Ni. $NiO_x$ film thickness: 1.2 μm; electrolyte composition: 0.5M $LiClO_4$ in propylene carbonate; scan rate: 40 mV $s^{-1}$. Black arrows indicate the direction of potential scan. The voltammetry shown is obtained after 250 cycles of stabilization.

The reduction of nanoporous $NiO_x$ coatings prepared via wet chemical methods, e.g. sol-gel, present voltammetry profiles similar to those of microblast, but with the exchange of lower current densities in anhydrous conditions.[14b] The cathodic process of lithium cations intercalation described in Eq.(1) is observed for Sample B within the potential range of 1.3-2.6 V *vs* $Li^+/Li$. Similar to the Sample **A** coating (Figure 7), the onset of the reduction of sintered $NiO_x$ nanoparticles (sample **B**) occurs at approximately 2.6 V.[9,47] However, the cathodic current density exchanged by

Sample **B** for the $NiO_x$ reduction [potential range 1.3 -2.6 V *vs* $Li^+/Li$ (Figure 8)], is generally lower than that obtained for sample **A** (Figure 7). Despite the larger surface area of $NiO_x$ electrodes obtained for sample **B, (**Figure 4b),[55-58] and for sol-gel deposited coatings,[6b,14b] the current density associated with $NiO_x$ reduction [Eq. (1)] is approximately two times higher for the microblast deposited sample **A**, which possesses a larger particle size in the order of several microns (Figure 2). This finding implies that lithium uptake accompanying the electrochemical reduction of these $NiO_x$ coatings [Eq. (1)] is not controlled by the surface area or by the mesoporosity of the electrodes.[59] It is more likely that current density is controlled by bulk characteristics such as the more ordered structure of $NiO_x$ of the microblast deposited coatings (Figure 6),[60] and, consequently, higher electron mobility and higher diffusion lengths within the larger grains of the microblast sample with respect to the sintered nanoparticles of the same material or nanoporous sol-gel deposits.[6b,14b] In addition to that, intraparticle charge transfer properties of semiconductor nanoparticles (sample **B**) may be affected by quantum confinement effects,[61] which are not relevant in microblast sample **A**. Moreover, the better uniformity of the metal oxide coverage on Ni substrate achieved with the microblast technique (Figure 4), brings about a stronger adhesion and improved charge transfer properties at the $Ni/NiO_x$ interface[62] in microblast samples when compared to the nanoparticle based films with nanoporous morphology.[23,25,41]
The effect of irradiation of bare and dye modified Sample **A** type coatings with white light was also investigated. The results obtained show that the electrochemical behaviour of these coatings is affected by irradiation as shown by an increase of the current density exchanged by the microblast sample in passing from the dark to the illuminated state within the potential range 1.2 - 3.2 V *vs* $Li^+/Li$ (Figure 9).

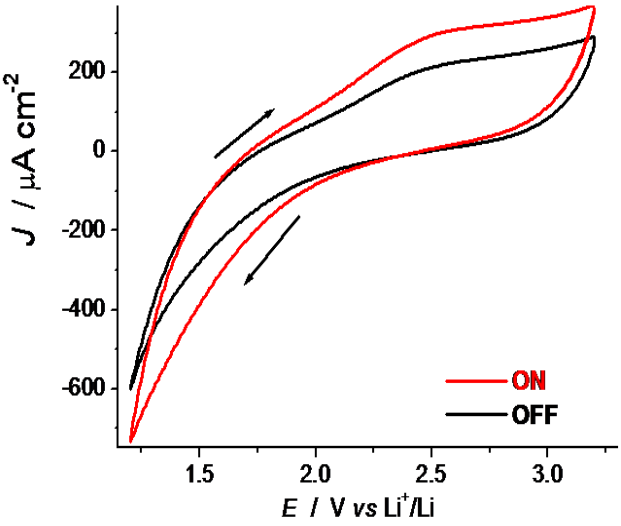


**Figure 9:** Cyclic voltammograms of sample A coating (thickness: 1.2 μm) obtained in dark (black line) and under frontal illumination (electrolyte side, red line). Light source was a halogen lamp (white light) with $P$ = 500 W. The arrows indicate the direction of scan. Scan rate: 100 mV $s^{-1}$.

The fact that the potential values at which current peaks are observed do not shift upon sample illumination suggests that the nature of the redox process associated with the current profiles of Figure 9 is not altered by visible light irradiation. Under identical conditions the charge exchanged during $NiO_x$ reduction is 2.78 and 2.82 mC $cm^{-2}$ in dark and illuminated sample **A**, respectively. The extent of reversibility defined as the ratio of the intercalated charge to the reverse extracted charge is 0.91 and 1 in the dark and upon illumination, respectively. The absence of any additional light-induced redox processes indicates that the microblast deposited semiconductor is photochemically stable.[63,64]

Sample A coatings were sensitized with Erythrosin B (ERY) dye as outlined in the experimental part.[41] The sensitization of the ERY-modified $NiO_x$ coatings was achieved as verified by the increase of optical absorption in the visible spectrum in passing from bare $NiO_x$ coating to its ERY-sensitized version (Figure 10). Spectra were taken in the reflectance mode with an integrating sphere due to the non-transparency of the oxide coatings on Ni substrate (Figure 3a).

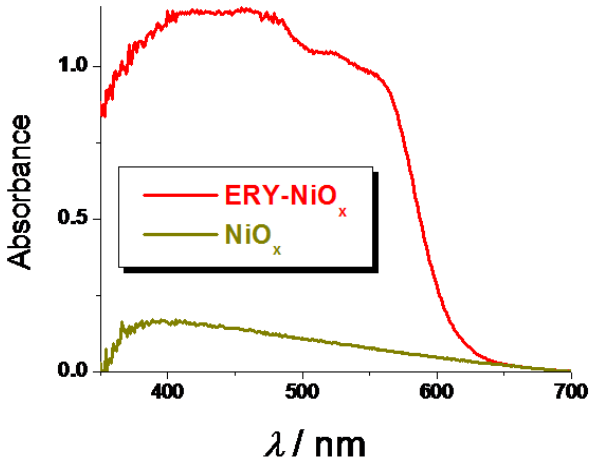


**Figure 10:** Absorption spectra of bare $NiO_x$ and ERY-sensitised $NiO_x$. Spectra were determined in the reflectance mode.

The electrochemical properties of the ERY/$NiO_x$ assembly are significantly altered (Figure 11) when compared with those of bare $NiO_x$ (Figure 7). The single cathodic wave displayed by the ERY-modified $NiO_x$ electrode, is observed at *ca*. 0.48 V *vs* $Li^+$/Li, i.e. approximately 1200 mV less positive than the value corresponding to the reduction of unmodified $NiO_x$ (1.67 V *vs* $Li^+$/Li, Figure 7).

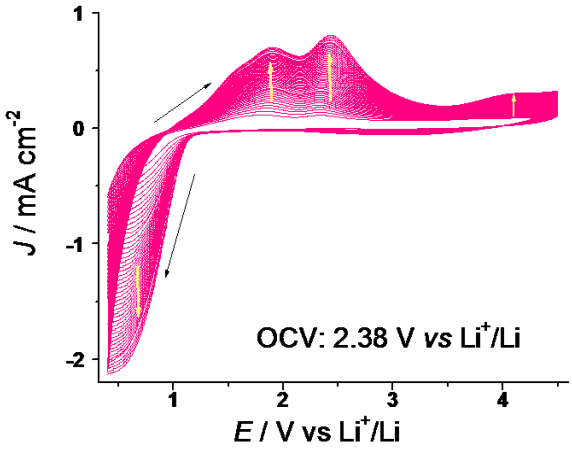


**Figure 11:** Cyclic voltammetry of dye-sensitized Sample A (thickness of the bare $NiO_x$ film: 1.2 μm). Electrolyte: 0.5M $LiClO_4$ in anhydrous propylene carbonate; scan rate: 40mV $s^{-1}$. Black arrows indicate the direction of potential scan. Yellow arrows show the direction of variation of the various current peaks with cycling.

This finding indicates the the ERY layer passivates the reduction of $NiO_x$ [Eq.(1)]. On the reverse scan two main anodic waves appear at 1.87 and 2.42 V *vs* $Li^+$/Li, whereas a third anodic wave is located at approximately 4.10 V *vs* $Li^+$/Li (Figure 11). The third anodic wave is associated with $NiO_x$ oxidation[55] as observed for the non-modified microblast $NiO_x$ samples (not shown). Electrochemical cycling of ERY-modified $NiO_x$ within the potential range 0.40 -4.50 V *vs* $Li^+$/Li (scan rate: 40 mV $s^{-1}$) brings about a continuous increase of the amount of exchanged charge during the first hundred cycles. After approximately 150 cycles the cyclic voltammetry stabilizes. The redox process that generates the cathodic wave at 0.48 V *vs* $Li^+$/Li is ascribed to the reduction of the ERY molecules within the organic layer and the underlying $NiO_x$ coating with the simultaneous insertion of lithium cations in both ERY layer and $NiO_x$ film for charge compensation according to the process:

$$ERY_{film}/NiO_x + (z+y)e^- + (z+y)Li^+ \Phi (ERY)^{z-}{}_{film}Li_z/Li_yNiO_x \quad (2)$$

where *z* and *y* represent the negative charge trapped within the reduced ERY layer (not to be confused with the charge per molecule) and within the reduced $NiO_x$ coating, respectively.

Under these circumstances both ERY molecules and $NiO_x$ have to be considered as redox-active species in the solid state. The broad anodic peak centred approximately at 1.9 V *vs* $Li^+/Li$ is ascribed to the neutralization of the reduced ERY layer:

$$(ERY)^{z-}{}_{film}Li_z/Li_yNiO_x \Phi ERY_{film}/Li_yNiO_x + zLi^+ + ze^- \qquad (3)$$

Therefore, the modification of microblast $NiO_x$ with ERY dye introduces an additional redox process [Eq. (2)] with respect to bare oxide coating. The anodic peak at 2.42 V *vs* $Li^+/Li$ displayed by dye-modified $NiO_x$ coating (Figure 11) strongly resembles the one related to the oxidation of ERY-free $Li_yNiO_x$ at 2.44 V *vs* $Li^+/Li$ (Figure 7). For this reason, it is assigned to the same redox process of oxidation of lithiated nickel oxide [Eq. (1) from right to left].[9,47,54] The electrochemical behaviour observed for the dye modified electrode suggests that both ERY and $NiO_x$ are electroactive species and act as electrochemical capacitors.[65] The confinement of redox processes within the species constituting the electrode itself is justified because of the absence of redox-active species in solution in the electrolyte under the experimental conditions here adopted. This brings about the localization of the observed redox processes at the *p*-type oxide itself for the bare electrode [Eq.(1)] and at the whole $ERY/NiO_x$ assembly in the dye-sensitized version [Eq.(2)]. The uptake of cathodic charge in ERY-modified $NiO_x$ is considerably larger than that of bare $NiO_x$ (18.75 *vs* 2.79 mC $cm^{-2}$, respectively). If it is assumed that the uptake of negative charge in reduced $NiO_x$ coating is the same in both bare and modified states, i.e. 2.79 mC $cm^{-2}$, the amount of cathodic charge stored solely in the ERY layer is 15.96 mC $cm^{-2}$, i.e. about six times larger than that of $NiO_x$. This is equivalent to say that the relative charge distribution within the two electroactive species ERY and $NiO_x$ expressed as the ratio *z*/*y* [Eq.(2)] will be approximately 6:1. If we consider that each molecule of ERY in the sensitizing layer exchanges one electron during the reduction process at 0.48 V *vs* $Li^+/Li$, the surface concentration of reduced ERY molecules will be about $1.6*10^{-7}$ moles $cm^{-2}$. The reduction process at 0.45 V *vs* $Li^+/Li$ (Figure 11) is diffusion controlled as proved by the linear dependence of the cathodic peak height at 0.45 V *vs* $Li^+/Li$ on the square root of the scan rate (Figure 12).[48]

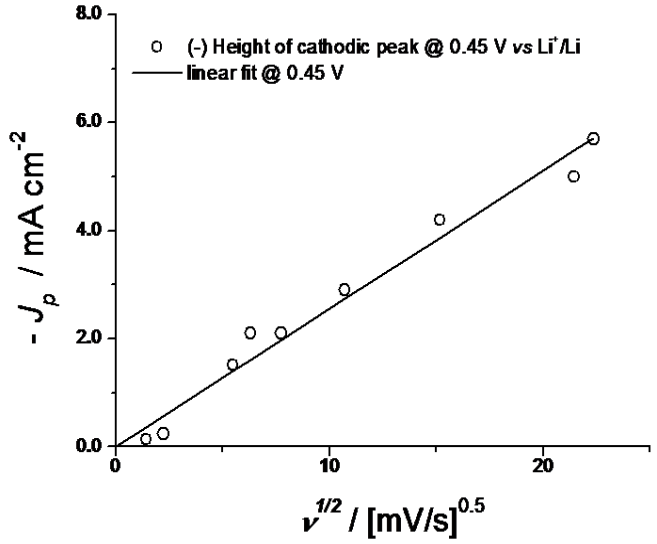


**Figure 12:** Plot of the cathodic current peak ($-J_p$) at 0.45 V *vs* $Li^+/Li$ versus the square root of scan rate ($v$) for the cyclic voltammetries of ERY-sensitised $NiO_x$ coating in the dark state. The cathodic peak refers to the electrochemical process of reduction described in Eq.(2).

This observation suggest the presence of an electroactive layer of dye, the reduction of which is controlled by the diffusion of charge carriers (both electronic and ionic) within the ERY-sensitised $NiO_x$ coating.[66] Since no shifts of potential are observed for the various current peaks in the cyclic voltammograms of the dye-sensitized $NiO_x$ surfaces upon irradiation, as already observed for the bare electrode, it can be concluded that the nature of the redox processes observed is not changing with illumination (Figure 13). Furthermore, no new voltammetric peaks are introduced in the cyclic voltammetry of dye-sensitized $NiO_x$ coating by visible light irradiation. The latter finding is again an indication of the photostability of the $NiO_x$ electrode also in the ERY-sensitized version (*vide supra*).

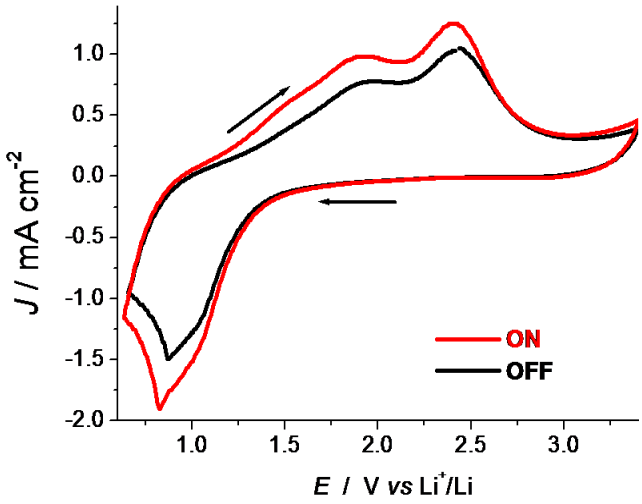


**Figure 13:** Cyclic voltammetries of dye-sensitized $NiO_x$ coating in dark (black line) and under illumination (red line). Scan rate: 40 mV $s^{-1}$. The light source was a white halogen lamp with $P$ = 500 W. Arrows indicate the direction of potential scan.

Therefore, the main effect of the illumination on ERY-sensitized microblast deposited $NiO_x$ consists of an increase of the current exchanged in reduction of the ERY-sensitized $NiO_x$ electrode [Eq.(b)]. Time integration of the cathodic current in Figure 13 gives 22.33 mC $cm^{-2}$ of charge density collected during the cathodic scan of ERY-modified microblast $NiO_x$ coating upon irradiation with visible white light. This value is larger than the charge uptake of ERY-modified $NiO_x$ coating in the dark state (18.75 mC $cm^{-2}$, *vide supra*). Such a difference is attributed to the increase of the density of mobile charge carriers following charge photo-injection, and of their mobility (thermal effect) within the illuminated ERY-modified $NiO_x$ electrode.

**Conclusions**

The objective of this study is to evaluate the use of the microblast technique for the preparation of NiOx thin film electrodes directly from the oxide powder without any thermal treatments. Microblast technique is a novel deposition method for the preparation of NiOx coatings to be employed eventually as p-type semiconductors in photoelectrochemical cells. The deposition of NiOx coatings at a high processing rate (20 mm2 s−1) without the need of thermal treatment has been demonstrated. The latter feature is particularly important for reducing the cost of time and energy to deposit such coatings. Based on these data films with area of 10 cm2 can be prepared in less than one minute. Moreover, the placed nozzle is close to the substrate surface which prevents any considerable loss of microblasted material during the deposition process. The morphology, crystal structure and chemical composition of the microblast deposited NiOx coatings deposited onto Ni sheets have been examined. The electrochemical reduction of microblast deposited NiOx coatings has been studied and compared with that of NiOx nanoparticulate layers obtained with a process of spraying/sintering, and with that of sol–gel deposited samples from literature data. A twofold increase in cathodic photocurrents was observed for the case of the microblast deposited NiOx coatings compared with nanoparticulate coatings of similar thickness but higher porosity (as evidenced by SEM analysis), when the electrochemical process of NiOx reduction in anhydrous environment with lithium electrolyte was considered. We found that this process is diffusion controlled. The larger currents of denser microblast NiOx with respect to more porous systems was ascribed to several factors: the higher diffusion length within the larger grains of the microblast deposited coatings with respect to the sintered nanoparticles of the same material, the charge transfer properties at the Ni/NiOx interface that improve in passing from nanoparticles films with mesoporous features to the microblast samples

due to the absence of empty zones at the Ni/NiOx interface. These results indicate that microblast procedure leads to an enhancement of the conductivity between NiOx grains, and good interfacial contact between the Ni substrate and NiOx coatings with respect to mesoporous NiOx samples prepared via sintering of nanoparticles, sol–gel methods or electrodeposition. XPS and XRD data on lithiated microblast NiOx show little compositional variation in passing from bare NiOx to the lithiated version when the range of potential 1.25–3.25 V vs Li+/Li was examined. Further experiments are still required for a complete structural analysis of the microblast NiOx coatings in the reduced state following the uptake of lithium cations at maximum capacity in order to evaluate the feasibility of microblast technique as preparation method of NiOx electrodes for lithium batteries. The photo-electrochemical behavior of microblast NiOx has been also analyzed and photoconduction effects have been observed.

**Acknowledgments**
M.A., D.D., D.P.D., and J.G.V. wish to acknowledge the financial support from Science Foundation Ireland (Project No. 07/SRC/B1160). Authors thank Prof. Valeria Di Castro (Dept. of Chemistry, University of Rome "La Sapienza") for her helpful comments during the analysis of XPS data.

**References**

1 .S.M. Wilhelm and N. Hackerman, *J. Electrochem. Soc.* 1981, **128**, 1668-1674.
2. S.R. Morrison, *Electrochemistry at semiconductor and oxidized metal electrodes*. Plenum Press, New York, 1980.
3. H. Sato, T. Minami, S. Takata and T. Yamada, *Thin Solid Films* 1993, **236**, 27-31.
4. C.G. Granqvist, *Sol. Energy Mater. Sol. Cells* 2007, **91** , 1529-1598.
5. S.P. Mitoff *J. Chem. Phys.* 1961, **35**,882-889
6. (a) K.W. Nam, W.S. Yoon and K.B. Kim, *Electrochim. Acta* 2002, **47**, 3201-3209; (b) K.C. Liu and M.A. Anderson, *J. Electrochem. Soc.* 1996, **143**, 124-130.
7. S.H. Lee, C.E. Tracy and J.R. Pitts, *Electrochem. Solid State Lett. A* 2004, **7**, A299-A301.
8. J.W. Lang, L.B. Kong, M. Liu, Y.C. Luo and L. Kang, *J. Solid State Electrochem.* 2010, **14**, 1533-1539.
9. (a) F. Decker, S. Passerini, R. Pileggi and B. Scrosati, *Electrochim. Acta* 1992, **37**, 1033-1038; (b) A. Surca, B. Orel and B. Pihlar, *J. Sol-Gel Sci. Techn.* 1997, **8**, 743-749.
10. K. Yoshimura, T. Miki and S. Tanemura, S *Jpn. J. Appl. Phys. Part 2* 1995, **34** , 2440-2446.
11. W.C. Yeh, and M. Matsumura, *Japanese . J. Appl. Phys. Part 1* 1997, **36**, 6884-6887.
12. (a) A. Azens, L. Kullman, G. Vaivars, H. Nordborg and C.G.Granqvist, *Solid State Ionics* 1998, **113-115**, 449-456; (b)F. Svegl, A. Surca Vuk, M. Hajzeri, L. Slemenik Perse, B. Orel *Sol. Energy Mater. Sol. Cells* 2012, **99**, 14-25.
13. Y. Sato, M. Ando and K. Murai, *Solid State Ionics*, 1998, **113-115**, 443-447.
14. (a) Z. Jiao, M. Wu, Z. Qin, Z and H. Xu, *Nanotechn.* 2003, **14** , 458-461; (b) H. Huang, J. Tian, W.K. Zhang, Y.P. Gan, X.Y. Tao, X.H. Xia and J.P. Tu, *Electrochim. Acta* 2011, **56**, 4281-4286.
15. (a) A. Avendaño, A. Azens, G.A. Niklasson and C.G Granqvist, *Materials Science and Engineering: B* 2007, **138** , 112-117; (b) F. Svegl, B. Orel and V. Kaucic, *Solar Energy* 2000, **68**, 523-540.
16. X.H. Xia, J.P. Tu, J. Zhang, X.L. Wang, W.K. Zhang and H. Huang, *Nanotechnology* 2008, **46**, 465701.
17. D. Gillaspie, A. Norman, C.E. Tracy, J.R. Pitts, S.H. Lee and A. Dillon, *J. Electrochem. Soc.* 2010, **157**, H328-H331.
18. I.M. Chan, T-Y. Hsu and F.C. Hong, , *Appl. Phys. Lett.* 2002, **81** , 1899-1901.
19. M.D. Irwin, D.B. Buchholz, A.W. Hains, R.P.H.Chang and T.J. Marks, *Proc. Nat. Acad. Sci.* 2008, **105** , 2783-2787.
20. I. Hotový, J. Huran, L. Spiess, S. Hascik and V. Rehacek, *Sensors Actuators B* 1999, **57**, 147-152.
21. I. Hotový, J. Huran, L. Spiess, J. Liday, H. Sitter and S. Hascík, *Vacuum* 2002, **69**, 237-242.
22. M. Awais, M. Rahman, J.M.D. MacElroy, D. Dini, J.G. Vos and D.P. Dowling, *Surf. Coat. Techn.* 2011, **205**, S245-S249
23. J. He, H. Lindstrom, A. Hagfeldt and S.E. Lindquist, *J. Phys. Chem. B* 1999, **103**, 8940-8943.
24. A. Morandeira, G. Boschloo, A. Hagfeldt and L Hammarström, *J. Phys. Chem. B* 2005, **109**, 19403-19410.
25. A. Nakasa, H. Usami, S. Sumikura, S. Hasegawa, T. Koyama and E. Suzuki, *Chem. Lett.* 2005, **34**, 500-501.
26. A. Morandeira, G. Boschloo, A. Hagfeldt and L. Hammarström, *J. Phys. Chem. C* 2008, **112**, 9530-9537.
27. A. Morandeira, J. Fortage, T. Edvinsson, L. Le Pleux, E. Blart, G. Boschloo, A. Hagfeldt, L. Hammarström and F. Odobel , *J. Phys. Chem. C* 2008, **112**, 1721-1728.
28. S. Mori, S. Fukuda, S. Sumikura, Y. Takeda, Y. Tamaki, E. Suzuki and T. Abe, *J. Phys. Chem. C* 2008, **112**, 16134-16139.
29. A. Nattestad, M. Ferguson, R. Kerr, Y-B Cheng and U. Bach, *Nanotechnology* 2008, **19**, 295304/1-9.
30. P. Qin, H. Zhu, T. Edvinsson, G. Boschloo, A. Hagfeldt and L. Sun, *J. Am. Chem. Soc.* 2008, **130** , 8570-8571.
31. E.A. Gibson, L.S. Amanda, L. Le Pleux, J. Fortage, G. Boschloo, E. Blart, Y. Pellegrin, F. Odobel, A. Hagfeldt and L. Hammarström, *Angew. Chem. Int. Ed.* 2009, **48**, 4402-4405.
32. M. Awais, M. Rahman, J.M.D. MacElroy, N. Coburn, D. Dini, J.G. Vos and D.P. Dowling, *Surf. Coat. Techn.* 2010, **204** , 2729-2736.

33. L. Li, E.A. Gibson, P. Qin, G. Boschloo, M. Gorlov, A. Hagfeldt and L. Sun, *Adv. Mater.* 2010, **22**, 1759-1762.
34. A. Nattestad, A.J. Mozer, M.K.R. Fischer, Y.B. Cheng, A. Mishra, P. Bauerle and U. Bach, *Nature Mater.* 2010, **9**, 31-35.
35. F. Odobel, L. Le Pleux, Y Pellegrin and E. Blart, *Acc. Chem. Res.* 2010, **43**, 1063-1071.
36. M.S. Wu and M.J. Wang, *Chem. Commun.* 2010, **46** , 6968-6970.
37. B. Hoghooghi and R. Raj, *J. Amer. Cer. Soc.* 1996, **79**, 1019-1024.
38. S.M. Pawar, B.S. Pawar, J.H. Kim, OS. Joo and C.D. Lokhande, *Curr. Appl. Phys* 2011, **11**, 117-161.
39. H.S. Kim, C.S. Kim and S.G. Kim, *J. Non-Cryst. Solids* 2006, **352**, 2204-2212.
40. I.A. Garduño, J.C. Alonso, M. Bizarro, R. Ortega, L. Rodríguez-Fernández and A.Ortiz, *J. Cryst. Growth* 2010, **312**, 3276-3281.
41. J. He, H. Lindström, A. Hagfeldt and S.E. Lindquist, *Sol. Energy Mater. Sol. Cells* 2000, **62**, 265-273.
42. Y. Mizoguchi and S. Fujihara, *Electrochem. Solid-State Lett.* 2008, **11**, K78-K80.
43. L. O'Neill, C. O'Sullivan, P. O'Hare, L. Sexton, F. Keady and J. O'Donoghue, *Surf. Coat. Techn.* 2009, **204**, 484-488.
44. P. O'Hare, B.J. Meenan, G.A. Burke,G. Byrne,D. Dowling and J.A. Hunt, *Biomaterials* 2010, **31**, 515-522.
45. Espe; 3M, *Scientific product profile/ Rocatec® bonding, Scientific Affairs* 12/2001.
46. J. Halme, J. Saarinen and P. Lund, *Sol. Energy Mater. Sol. Cells* 2006, **90** , 887-899.
47. (a) S. Passerini and B. Scrosati, *J. Electrochem. Soc.* 1994, **141**, 889-895; (b) S. Passerini, B. Scrosati and A. Gorenstein, *J. Electrochem. Soc.* 1990, **137**, 3297-3300.
48. A.J. Bard and L.R. Faulkner, *Electrochemical Methods: Fundamentals and Applications*. 2nd ed.; John Wiley & Sons: New York, 2001.
49. M. Raffel, C. Willert and S. Wereley, *Particle image velocimetry: A practical guide*. Springer Verlag: 2007.
50. E. Avvakumov, M. Senna and N. Kosova, *Soft mechanochemical synthesis: A basis for new chemical technologies*. Springer Netherlands: 2001.
51. S.J. Klaine, P.J.J. Alvarez, G.E. Batley, T.F. Fernandes, R.D. Handy, D.Y. Lyon, S. Mahendra, M.J. McLaughlin and J.R. Lead, *Environ. Toxic. Chem.* 2008, **27**, 1825-1851.
52. (a) S. Uhlenbrock, C. Scharfschwerdt, M. Neumann, G. Illing and H.J. Freund *J. Phys. Condens. Matter* 1992, **4**, 7973-7978; (b) A. Davidson, J.F. Tempere, M. Che, H. Roulet and G. Dufour, *J. Phys. Chem.* 1996, **100**, 4919-4929.
53. C.H. Hager Jr, J. Sanders, S. Sharma, A. Voevodin and A. Segall, *Tribology International* 2009, **42**, 491-502.
54. M.S. Whittingham, *J. Electrochem. Soc.* 1976, **123**, 315-320.
55. G. Boschloo and A. Hagfeldt, *J. Phys. Chem. B* 2001, **105**, 3039-3044.
56. R. Jose, V. Thavasi and S. Ramakrishna, *J. Am. Cer. Soc.* 2009, **92** , 289-301.
57. M. Boucharef, C.D. Bin, M.S. Boumaza, M. Colas; H.J. Snaith, B. Ratier and J. Bouclé, *Nanotechnology* **2010**, 21, 205203/1-12.
58. H.G. Jung, Y.S. Kang and Y.K. Sun, *Electrochim. Acta*, 2010, **55** , 4637-4641.
59. E.L. Miller and R.E. Rocheleau, *J. Electrochem. Soc.* 1997, **144** , 3072-3077.
60. I.C. Faria, M. Kleinke, A. Gorenstein, M.C.A. Fantini and M.H. Tabacniks, *J. Electrochem. Soc.* 1998, **145**, 235-240.
61. A. Hagfeldt and M. Grätzel, *Chem. Rev.* 1995, **95**, 49-68.
62. D. Jeong, W. Kim, Y. Choi and Y. Sung, *J. Electroanal. Chem.* 2001, **511**, 79-87.
63. H. Gerischer, *Ann. Rev. Phys. Chem.* 1961, **12**, 227-254.
64. H. Gerischer and F. Willig, *Topics in Current Chemistry* 1976, **61**, 31-84.
65. G.A. Snook, P.Kao and A.S. Best, *J. Power Sources* 2011, **196**, 1-12.
66. A.Tarola, D. Dini, E. Salatelli, F.Andreani and F.Decker, *Electrochim. Acta* 1999, **44**, 4189-4193.